SUPPORTING INFORMATION APPENDIX

Cardiac electrical defects in progeroid mice and Hutchinson-Gilford progeria syndrome patients with nuclear lamina alterations

José Rivera-Torres, Conrado J. Calvo, Anna Llach, Gabriela Guzmán-Martínez, Ricardo Caballero, Cristina González-Gómez, Luis J. Jiménez-Borreguero, Juan A. Guadix, Fernando G. Osorio, Carlos López-Otín, Adela Herraiz-Martínez, Nuria Cabello, Alex Vallmitjana, Raul Benítez, Leslie B. Gordon, José Jalife, José Mª Pérez-Pomares, Juan Tamargo, Eva Delpón, Leif Hove-Madsen, David Filgueiras-Rama, Vicente Andrés

GLOSSARY OF ELECTROCARDIOGRAPHIC PARAMETERS

Bradycardia (in mice): A heart rate slower than normal average values in mice using the same protocol for anesthesia. Average heart rate in mice anesthetized with isoflurane (like in the present studies) has been previously reported at 450±17 bpm (1, 2), therefore bradycardia in our studies is considered at heart rates below such values.

Bradycardia (in children >3 years of age): A heart rate <60 bpm.

P wave: First positive deflection observed in the ECG, representing atrial depolarization.

PQ interval: Time between the beginning of atrial depolarization and the beginning of ventricular depolarization.

PR interval: Time from the onset of the P wave to the start of the QRS complex; it mainly reflects conduction through the AV node.

Q wave: Any negative deflection that precedes an R wave.

QRS: Series of deflections in an electrocardiogram that represent electrical activity generated by ventricular depolarization.

QT interval: Time from the start of the Q wave to the end of the T wave.

QTc: Duration of the QT interval corrected for the patient's heart rate.

R wave: The initial upward deflection of the QRS complex, after the Q wave; it represents ventricular depolarization.

RR interval: Time between two consecutive R waves in the electrocardiogram; it represents a complete cardiac cycle (patient's heart rate).

ST segment: The flat, isoelectric section of the ECG between the end of the S wave and the beginning of the T wave.

T wave: Electrocardiogram deflection that represents the electrical activity produced by ventricular repolarization.

SI MATERIALS AND METHODS

Electrocardiographic analysis of human ECG. Standard ECG recordings from human age-matched controls volunteers and HGPS patients were used to assess differences in repolarization abnormalities. Lead II and precordial V5 traces, commonly used for diagnosis of repolarization abnormalities (3) were selected to assess temporal and morphological differences between controls and patients, at the initial follow-up and advanced stages of the disease (last follow-up).

A semi-automatic approach was used for digitization using a Matlab-based custom tool **(Supplemental Figure S13)**, as previously described (4). Briefly, ECG recordings were scanned to a digital image (600 dpi) and stored in a codified digital format. To identify ECG traces on the standard ECG-paper, image-processing techniques were applied involving binary thresholding, pixel-to-point conversion and transform techniques. When necessary, images were pre-processed to avoid artifacts (contrast, median filtering and interpolation) in the digitization process. Pixel-to-point conversion was applied using the lower waveform envelope. The graphical grid was used as reference for interpretation.

Corrected QT interval (QTc) was calculated using Bazett's formula, and considered prolonged when >450 ms for men and >470 ms for women (5). Age-dependent effects on human repolarization variability were quantified from averaged ECGs extracted from standard paper-ECG lead II **(Supplemental Fig.S13).** Human repolarization alterations were quantified using a rate-independent T-wave flattening score obtained from averaged area-normalized T-waves and compared with age-matched controls **(Supplemental Fig.S13)** (6). The human T-wave Flattening Score was compared with ECG traces from age-matched healthy controls. The formulation applied is described below:

$$Human\,T_{wave}\,Flattening\,Score = \left(1 - \frac{\sqrt[4]{M_4}}{0.1 \cdot M_2^2}\right)$$

$$where:$$

$$M_k = \frac{\left[\sum_{i=1}^{n} (x_i - \bar{x})^k \cdot T(i)\right]^{\frac{1}{k}}}{Var\_T^2};$$

where T wave flatness is obtained for the unit area normalized T-wave. We used a modified and corrected peakedness factor described by the 4^{th} central moment normalized to the variance. The score was corrected to allow increasing values of flatness reflect increasing values of flattening of the T-wave.

All data analyses, extraction and quantifications were done using custom scripts written in MATLAB software (version 8.1 release R2013a, The MathWorks Inc, Natick, Massachusetts, USA).

Beat-to-beat variability of the RR interval series was primarily assessed using 2-dimensional representations of the pairs RR_n-RR_{n+1} (n=cardiac beat number within the entire registration period) color-coded for time from blue to red.

Time-course electrocardiographic analysis of mouse cardiac rhythm abnormalities. Mice were anesthetized with 1.5-2% isoflurane in oxygen, inhaled through a facial mask. To avoid night-day circadian variations, ECG was performed in the morning. ECG electrodes were inserted subcutaneously in the four limbs and sequential ECG recordings were acquired at 2 KHz sweep-speed using a MP36R data acquisition workstation (Biopac Systems). Data were stored for off-line analysis using custom

MatLab scripts. From 11 weeks of age (First week) until 19 weeks of age or death of the animal (Last week), *Zmpste24*$^{-/-}$ and wild-type mice were given weekly β-adrenergic challenge with isoproterenol (i.v. bolus 0.34 mg/kg). ECG traces were recorded at baseline, after challenge, and during recovery (10 to 25 min).

ECG recordings were analyzed offline using custom scripts for pre-processing, visualization and quantification of electrophysiological intervals and heart rate variability markers. After band-pass filtering between 0.5-250 Hz, baseline wander was removed using a bidirectional filtering strategy. Baseline drift removal is essential for morphological analysis of T-waves. **Supplemental Figure S4** shows averaged ECG from WT and *Zmpste24*$^{-/-}$ mice obtained after Q-wave alignment from up to 100 beats in mice at baseline, prior to β-adrenergic stimulation. Specifically: i) PR intervals were measured from the beginning or the P wave to the peak of the R wave; ii) QRS intervals were measured from the beginning of the Q wave until the point where the S wave crosses the baseline; and iii) QT intervals were measured from the beginning of the Q wave until the point where the T-wave declines to 90% (T_{90}) from the peak (7). Finite differential methods and wavelet transform were used for fiducial point estimation. R-peak detection was robustly estimated by parabolic fitting of the coiflet wavelet transform and detection of the maximum magnitude point. All R detections were supervised to ensure accuracy of ECG segmentations. After QRS detection, P and T wave segments were extracted using adaptive windowing depending upon beat-to-beat RR changes. After segmentation using differential methods, both waves were low-pass filtered at 20 Hz using a Kaiser window FIR filter.

Adaptive heart-rate-corrected QT values (QTc) were derived using a modification of Bazzet's formula for murine electrocardiography (8). RR and QTc dispersion were assessed as the difference between the maximum and minimum intervals measured. Up to 5 minutes of recordings, aligned to the Q-wave, were used to obtain signal-averaged ECG (SAECG) traces, where additional electrophysiological parameters were quantified for data analyses. Quantified variables were mean P-wave duration, QRS duration, T-wave duration and dispersion, Q-wave to T_{peak}, and T_{peak} to T_{90} (90% of repolarization from T_{peak}) (not shown). All measured intervals were based on previous studies in murine electrophysiology (9).

T-wave morphological alterations were quantified by defining a modified flattening kurtosis-based descriptor derived for mice (6) **(Supplemental Figure S14).** T-wave SAECG in each segment of interest (up to 5 minutes, 2143±274 complexes) was considered for T-wave parameterization. SAECG traces were appropriately de-trended and rectified to determine the T-wave onsets. T-wave offset was determined as the 90% repolarization from the T-wave peak (T_{90}). T-wave end (T_{end}) was defined as the maximum change in slope during recovery to the isoelectric line. T-waves were interpreted as unit-area normalized probability density functions (TPDFs) for kurtosis estimation to describe the peakedness of the distribution as compared to a Gaussian distribution function. The flattening score was defined as the product of a geometric factor multiplied by the inverted normalized kurtosis corrected to achieve increasing values of flattening score with increasing flatness of the T-wave. The equation applied is:

$$Mice\,T_{Wave}\,Flattening\,Score = 0.25 \cdot \left[\frac{(1 - \frac{\sqrt[4]{M_4}}{M_2^2}) \cdot (1 - \left[\frac{T_d}{T_p - T_{on}} \right]^{\frac{1}{2}})}{1 + dTdt_{\max} \cdot A_T^2} \right]^{\frac{1}{4}}$$

where the peakedness factor is described by the central moments used to obtain excess kurtosis (fourth central moment normalized to the squared second moment) of the TPDFs were calculated as described elsewhere (10). A geometrical correction factor includes T_d and T_p-T_o as the averaged T-wave duration and the T elevation from the isoelectric line. A_T represents the area prior to normalization and $dTdt_{max}$ the T-wave upstroke depolarization. **Supplemental Figure S14** shows representative traces of SAECGs with corresponding segmented T-waves and flattening score values for *Zmpste24*$^{-/-}$ and wild-type mice in each segment of interest for the initial (First; 11 week) and last week of follow-up.

All the above-described ECG measures were quantified in *Zmpste24*$^{-/-}$ mice and controls at baseline (1 minute), after ß-adrenergic stimulation to exacerbate the *Zmpste24*$^{-/-}$ phenotype (5 minutes), and during recovery (4 minutes). Any premature ventricular complexes (PVC) or spontaneous ventricular rhythms were quantified and classified as isoproterenol-related or bradycardia-related.

Heart rate variability analysis in mice. We quantified short and mid-term heart rate variability (HRV) markers from ECG recordings of up to 25 min. Time domain, frequency domain geometrical and non-linear standard HRV descriptors (11) were automatically quantified using custom scripts in Matlab. All R-waves detected were considered for the offline heart rate variability analysis. A mean of 5739±1402 complexes was considered in each animal. Time domain descriptors included the mean and standard deviation of the RR interval series, as well as descriptors for quantification of beat-to-beat rate differences.

Mouse transthoracic echocardiography. Two-dimensional and M-mode echocardiography studies were performed weekly in anesthetized mice (1.5-2% isoflurane in a mixture with oxygen by a facial mask) using a Vevo 770 system (VisualSonic) equipped with a 30-MHz linear transducer probe. To avoid night-day circadian variations, echocardiography was performed in the morning. Before echocardiography, animal fur was removed with a topical depilatory agent and animals were warmed to maintain body temperature. The heart was imaged in the 2D parasternal long- and short-axis projections with guided M-mode recordings at the midventricular level in both views. LV end-diastolic diameter (LVEDD), LV-systolic diameter (LVESD), end-diastolic LV anterior wall thickness (LVAW), and LV posterior wall thickness (LVPW) were measured from images obtained by M-mode echocardiography. LV fractional shortening (FS) was calculated as follows:

$$FS\ (\%) = [(LVEDD-LVESD)/LVEDD][100].$$

LV ejection fraction (EF) and LV mass were calculated as follows:

$$EF\ (\%) = [(LVEDD3-LVESD^3)/LVEDD^3][100]$$

$$LV\ mass\ (mg) = [1.053][(LVEDD + LVAW + LVPW)^3 - (LVEDD)^3]$$

Blood pressure measurements in mice. A noninvasive automated tail-cuff device was used (Visitech System BP2000, NC). Mice were trained on a daily basis for one week, and weekly measurements were made at the same time in the morning. For greater accuracy, the first 10 of 20 measurements were discarded, and mean of the last 10 measurements were used for analysis.

Histomorphologic characterization of mouse heart. *Zmpste24*$^{-/-}$ and wild-type hearts were fixed in 4% paraformaldehyde, embedded in paraffin, sectioned with a microtome (10μm) and mounted on poly-L-lysine-coated glass slides. Routine histological analysis was performed using picrosirius red and Mallory's trichrome staining.

Coronary artery fibrosis was quantified in Mallory's trichrome-stained sections from 5 animals of each genotype. Large caliber arteries at the interventricular septum and free ventricular walls were identified and 3 transverse arterial profiles photographed along a total length of 300-400 μm (a minimal distance of 30 μm between sections was observed). Fibrosis was plotted against the total surface of the arterial medial wall using Adobe Photoshop, and the percentage of fibrotic pixels with respect to the total arterial surface was calculated with FiJi software. Statistical significance was assessed using t-Student's test by separately comparing each mutant specimen with a matched control, as well as by comparing pooled data from all mutants and wild-type specimens.

To quantify cardiomyocyte size, Mallory's-trichrome-stained left and right ventricular sections from 4 mice of each genotype were photographed with a NIKON DXM1200 camera. The profiles of individual cardiomyocytes were manually defined using Adobe Photoshop. The total area of each cardiomyocyte cross section (as an estimate of cell diameter/minor axis) was plotted as a black domain on a white background. Ninety cardiomyocytes were analyzed per ventricle (right/left) and specimen. NIH ImageJ software was used to quantify the total number of pixels per discrete black area (cardiomyocyte surface) in mice of both genotypes.

Autopsy specimens. Paraffin-embedded autopsy left ventricle specimens from HGPS patients HG028 and HG120 were obtained from the Cell and Tissue Bank of the Progeria Research Foundation (Rhode Island Hospital, Providence, RI) (www.progeriaresearch.org/cell_tissue_bank.html). Tissues were fixed in 2% paraformaldehyde and embedded in paraffin. Mutational analysis via the PRF Diagnostics Program (www.progeriaresearch.org/diagnostic_testing.html) identified the *LMNA* c.1824C>T mutation in both patients.

Immunohistochemistry. Mouse heart sections were immunostained using primary antibodies against smooth muscle α-actin (SMα-actin; SIGMA). Sections were dewaxed and rinsed with PBS. Endogenous peroxidase was quenched with 6% H_2O_2 and specimens were blocked in 1% BSA + 5% goat serum + 0.1% Triton X-100 for 3 h at room temperature. Slides were then incubated with primary antibody diluted in PBS (overnight, 4ºC), washed in PBS, and incubated with biotinylated anti-mouse smooth muscle α-actin for 3 h at room temperature. After washing in PBS, the samples were incubated in HRP-conjugated ExtrAvidin (SIGMA), and peroxidase activity was developed using the SIGMA Fast kit (Urea buffer + DAB). After final washes in water, specimens were dehydrated and mounted in DePeX (VWR BDH) for light microscopy inspection.

Double immunostaining for connexin 43 (Cx43) and N-cadherin (N-Cadh) was performed in left ventricular transverse-sections (10μm) from mice and HGPS patients HG028 and HG120 (see above "Autopsy specimens"). Antigens were retrieved by heating in TEG buffer (25 mM Tris-HCl pH 8, 10 mM EDTA 50 mM glucose) in a pressure cooker. Before primary IgG incubation, endogenous biotin was blocked using an avidin/biotin blocking kit (Vector Laboratories). Non-specific IgG binding was blocked with SBT solution (5% goat serum, 1% BSA and 0.5% Triton X-100 in Tris-PBS). Samples were incubated overnight (4ºC) with anti-Cx43 (1:50 in SBT, ABNOVA Anti-GJA1) and anti-NCadh (1:50 in SBT, DSHB-MNCD2). After extensive washes with PBS, sections were incubated for 2 h with biotinylated anti-rabbit IgG (1:100 in PBS), washed again in PBS, and incubated in TRITC-coupled extravidin and anti-mouse FITC for 2 h at room temperature. After final PBS washes, cell nuclei were counterstained with DAPI (1:2000 in PBS) and slides were mounted in Glicerol/PBS (1:1). Samples were visualized with a SP5 laser confocal microscope (LEICA).

Quantification of Cx43 mislocalization in heart sections. Image analysis of raw inmunohistochemical fluorescently-labeled mouse and human heart sections was performed to accurately quantify Cx43 localization at the intercalated disks. Extracted hyperstacks were separated into independent channels prior to image pre-processing. Two-dimensional median filtering with a

5x5 neighborhood was applied to minimize salt-and-pepper background noise. Semi-automatic segmentation by multidimensional histogram thresholding based on pixel intensities was applied to obtain binary feature extracted images and was corrected if necessary to optimize levels within each channel across heart sections. Additional morphological operations were applied for each individual binary mask, including filling, erosion and dilatation with a disk-shaped structuring element of radius = 4 pixels neighborhood to remove false positives. Detected blobs were delineated using a connectivity kernel of 8 pixels and used for binary image operations to determine staining and determine % co-localization among staining channels. A circularity score was defined as previously validated using ImageJ software (12). Cx43 was considered to be accumulated laterally when not co-localizing with the intercalated disks (N-Cadh) or internalized near the nuclei (co-localizing with DAPI), which simultaneously presented high (>0.5) circularity scores. All automatically segmented images were inspected by two independent investigators to validate the methodology.

Quantitative real-time PCR (qPCR). Total RNA was extracted from mouse heart apex tissue using QIAzol reagent (QIAGEN). cDNAs were synthesized using the SuperScript III First- Strand Synthesis System for RT-PCR (Invitrogen) and oligo dT primers. cDNA amounts were determined by qPCR using SYBR green qPCR Mix (Applied Biosystems). PCR conditions for amplification of all genes were 1 min at 95ºC and 40 cycles of 95ºC for 30 s, 57ºC for 30 s, and 72ºC for 30 s. Specificity of the SYBR green assays was confirmed by melting-point curve analysis. Expression data were calculated in qBASE from the cycle threshold (Ct) value using the ΔΔCt quantification method. Gene expression of 18S rRNA and GAPDH were used for normalization. Primers used for amplification are as follows:

GENE	Forward (5' – 3')	Reverse (5' – 3')
Orai1	AACGAGCACTCGATGCAGG	GGGTAGTCATGGTCTGTGTCC
STIM	TGACAGGGACTGTACTGAAGATG	TGCCGAGTCAAGAGAGGAGG
CSQ1	CTCATCAGCAGAAGGCAGGT	TTGACCTGTCAGCTCCACAA
CSQ2	TGCTCATGGTGGGGGTTTATC	AGGTTCGTGGTAATAGAGACAGA
SERCA2a	GAGAACGCTCACACAAAGACC	ACTGCTCAATCACAAGTTCCAG
RyR2	GCAGTCCCTGTCAGTACGG	CGTGTCCATAGAGGAGTGTCC
SCN5A	ATGGCAAACTTCCTGTTACCTC	CCACGGGCTTGTTTTTCAGC
KCND3	CCGGTCCCTGTGATAGTCTC	AGGGGATCATCCACAAGATAGG
KCNQ1	CGCGGTGGTCAAGAAGTGT	CACTGTAGATGGAGACCCG
KCNJ2	ATGGGCAGTGTGAGAACCAAC	TGGACTTTACTCTTGCCATTCC
KCNH2	GTGCTGCCTGAGTATAAGCTG	CCGAGTACGGTGTGAAGACT
KCNA5	TCCGACGGCTGGACTCAATAA	CAGATGGCCTTCTAGGCTGTG

Western blot. Mouse hearts were dissected, extensively washed with PBS and immediately snap-frozen in liquid nitrogen until further use. The hearts were ground with a mortar while frozen, further disrupted with TissueLyser (QIAGEN), and homogenized after incubation for 30 min at 4ºC with gentle rocking in lysis buffer (50 mM Tris-HCl pH 7.5; 0.1 M NaCl, 1 mM $MgCl_2$, 1 mM DTT, and 2% TX-100) supplemented with phosphatase and protease inhibitor cocktails (Roche). Protein concentration was determined by the Bradford assay (Protein Assay Kit, Bio-Rad). Cell extracts were preserved at -80ºC until use. For protein analyses, total protein extracts (40 µg) were mixed with Laemmli sample buffer (62.5 mMTris-HCl, pH 6.8, 2.3% SDS, 10% glycerol, 5% β-mercaptoethanol, 0.005% bromophenol blue), boiled for 10 min, and resolved on 10-12% SDS-polyacrylamide gels. Proteins were transferred to PVDF membranes using the iBlot Dry Blotting system (Invitrogen). Membranes were incubated for 1 h at room temperature in blocking buffer (5% non-fat dried milk in TBS, 0.2% Tween-20) followed by incubation with primary antibodies diluted in blocking buffer (overnight, 4ºC). Primary antibodies were purchased from Sigma-Aldrich (anti-

tubulin, ref. T9026), Invitrogen (anti-Cx43, ref. 71-0700), Abcam (anti-desmin, ref. ab8592; anti-CSQ, ref ab3516), Beckton Dickinson (anti-plakoglobin; ref BD610253), and Santa Cruz Biotechnology (anti-Serca2, ref sc8095). After washes with TBS, 0.2% Tween-20, membranes were incubated with appropriate HRP-conjugated secondary antibodies (Santa Cruz) for 1 h at room temperature, and specific proteins were visualized by enhanced chemiluminescence (GE Healthcare).

To quantify relative protein levels in heart, western blots were performed with heart extracts from 3 wild-type and 3 *Zmpste24*$^{-/-}$ mice. The intensity of protein bands was determined by densitometric analysis of independent blots for each lysate (2 blots for plakoglobin and SERCA2 and 3 blots for desmin, Cx43, and CSQ). Protein abundance was normalized to the intensity of the tubulin loading control. Mean values were first calculated for the methodological replicates from the 2-3 independent blots. These values were then used to calculate the overall mean value for each genotype. Results are presented as mean±SEM (relative to wild-type=1).

Action potential (AP) measurements in mouse ventricular preparations. Transmembrane APs were recorded in ventricular preparations from male wild-type and *Zmpste24*$^{-/-}$ mice using glass microelectrodes filled with 3 M KCl (tip resistance: 8-15 MΩ) (13). Multicellular preparations were perfused with a modified Tyrode's solution containing (in mM): NaCl 125, KCl 5.4, $CaCl_2$ 1.8, $MgCl_2$ 1.05, $NaHCO_3$ 24, NaH_2PO_4 0.42 and glucose 11. The solution was bubbled with 95% O_2 and 5% CO_2 (pH=7.4) and maintained at 34°C. The microelectrode was connected with Ag-AgCl wire to high-input impedance, capacity-neutralizing amplifiers (model 701; WPI, New Haven, CT, USA). Left ventricular preparations were stimulated using rectangular pulses (duration 1-2 ms) at a frequency of 3 Hz delivered from a multipurpose programmable stimulator (CS-220; Cibertec SA, Madrid, Spain). APs were computer stored using Acknowledge software. Recordings from at least three stable microelectrode impalements were stored for each preparation.

Intracellular calcium measurements in isolated mouse cardiomyocytes. Ventricular cardiomyocytes were isolated from mouse hearts by enzymatic digestion. Briefly, the heart was mounted on a Langendorf perfusion system and perfused at a constant flow rate of 3 ml/min. The heart was first perfused for 5 min with nominally calcium-free Tyrode's solution containing (in mM): NaCl 88, sucrose 78, KCl 5.4, $MgCl_2$ 1, HEPES 10, Na-pyruvate 5 and glucose 10 plus 2 mg/ml BSA. Subsequently, atria were removed and ventricles were digested for 8 min with nominally calcium-free Tyrode's solution containing collagenase (0.4 mg/ml, Worthington type II). To increase cardiomyocyte yield, additional digestion was carried out for 5 min in collagenase-containing calcium-free Tyrode's solution with gently agitation. This process was repeated three times and desegregated cardiomyocytes were pooled in a solution in which extracellular calcium concentration was increased stepwise to 0.2, 0.4, and 0.8 mM. Cardioyocytes were then stored at room temperature and those showing elongated and striated features were used for electrophysiological, calcium imaging and immunofluorescent labelling studies.

Confocal Ca^{+2} imaging was performed in fluo-4 loaded ventricular cardiomyocytes using a Leica TCS SP5 resonance scanning confocal microscope equipped with a 63X 1.3 NA glycerol objective. Fluo-4 was excited at 488 nm and fluorescence emission was measured between 500 and 650 nm in the frame scanning mode (14). Calcium transients were recorded at room temperature (20-22^{o}C) and elicited by subjecting cardiomyocytes to electrical field stimulation (5 ms pulses, 5-15 V) at increasing stimulation frequency (0.5 to 4 Hz). Calcium transients and spontaneous calcium waves were automatically detected and quantified using custom-made programs (15).

Perforated patch-clamp in mouse ventricular cardiomyocytes. Ionic currents in ventricular cardiomyocytes were measured with the perforated patch-clamp technique (16). L-type calcium

currents were elicited by a 100 ms depolarization to 0 mV from a holding potential of -80 mV. Na^+-currents were eliminated by inclusion of 30 μM tetrodotoxin in the bath solution and a 50-ms prepulse from -80 to -50 mV. Transient inward currents were measured with the holding potential clamped at -80 mV for 30s. The amount of calcium released from the SR was measured by rapid and transient treatment with 10 mM caffeine (with the membrane potential clamped at -80 mV during the 5 s of caffeine application) followed by integration of the elicited inward current.

Statistical analysis. Data are presented as mean ± SEM. Statistical significance was assessed by unpaired two-tailed t-test for comparisons involving two groups, or one-way ANOVA followed by Newman–Keuls post-hoc test for multiple comparisons. Statistical significance was assigned at $p<0.05$.

REFERENCES

1. Ho D, *et al.* (2011) Heart Rate and Electrocardiography Monitoring in Mice. *Curr Protoc Mouse Biol* 1:123-139.
2. Stypmann J (2007) Doppler ultrasound in mice. *Echocardiography* 24(1):97-112.
3. Monnig G, *et al.* (2006) Electrocardiographic risk stratification in families with congenital long QT syndrome. *Eur Heart J* 27(17):2074-2080.
4. Filgueiras-Rama D, *et al.* (2015) Spectral analysis-based risk score enables early prediction of mortality and cerebral performance in patients undergoing therapeutic hypothermia for ventricular fibrillation and comatose status. *Int J Cardiol* 186:250-258.
5. Priori SG, *et al.* (2013) HRS/EHRA/APHRS expert consensus statement on the diagnosis and management of patients with inherited primary arrhythmia syndromes: document endorsed by HRS, EHRA, and APHRS in May 2013 and by ACCF, AHA, PACES, and AEPC in June 2013. *Heart Rhythm* 10(12):1932-1963.
6. Andersen MP, *et al.* (2008) New descriptors of T-wave morphology are independent of heart rate. *J Electrocardiol* 41(6):557-561.
7. McLerie M & Lopatin AN (2003) Dominant-negative suppression of I(K1) in the mouse heart leads to altered cardiac excitability. *J Mol Cell Cardiol* 35(4):367-378.
8. Mitchell GF, Jeron A, & Koren G (1998) Measurement of heart rate and Q-T interval in the conscious mouse. *Am J Physiol* 274(3 Pt 2):H747-751.
9. Kaese S & Verheule S (2012) Cardiac electrophysiology in mice: a matter of size. *Front Physiol* 3:345.
10. Graff C, *et al.* (2009) Quantitative analysis of T-wave morphology increases confidence in drug-induced cardiac repolarization abnormalities: evidence from the investigational IKr inhibitor Lu 35-138. *J Clin Pharmacol* 49(11):1331-1342.
11. listed Na (1996) Heart rate variability. Standards of measurement, physiological interpretation, and clinical use. Task Force of the European Society of Cardiology and the North American Society of Pacing and Electrophysiology. *Eur Heart J* 17(3):354-381.
12. Schneider CA, Rasband WS, & Eliceiri KW (2012) NIH Image to ImageJ: 25 years of image analysis. *Nat Methods* 9(7):671-675.
13. Caballero R, *et al.* (2010) Flecainide increases Kir2.1 currents by interacting with cysteine 311, decreasing the polyamine-induced rectification. *Proc Natl Acad Sci USA* 107(35):15631-15636.
14. Llach A, *et al.* (2011) Sarcoplasmic reticulum and L-type Ca(2)(+) channel activity regulate the beat-to-beat stability of calcium handling in human atrial myocytes. *J Physiol* 589(Pt 13):3247-3262.
15. Barriga M, *et al.* (2013) Low density lipoproteins promote unstable calcium handling accompanied by reduced SERCA2 and connexin-40 expression in cardiomyocytes. *PLoS One* 8(3):e58128.
16. Hove-Madsen L, *et al.* (2004) Atrial fibrillation is associated with increased spontaneous calcium release from the sarcoplasmic reticulum in human atrial myocytes. *Circulation* 110(11):1358-1363.
17. Li L, *et al.* (2010) A mathematical model of the murine ventricular myocyte: a data-driven biophysically based approach applied to mice overexpressing the canine NCX isoform. *Am J Physiol Heart Circ Physiol* 299(4):H1045-1063.

SUPPLEMENTAL FIGURES

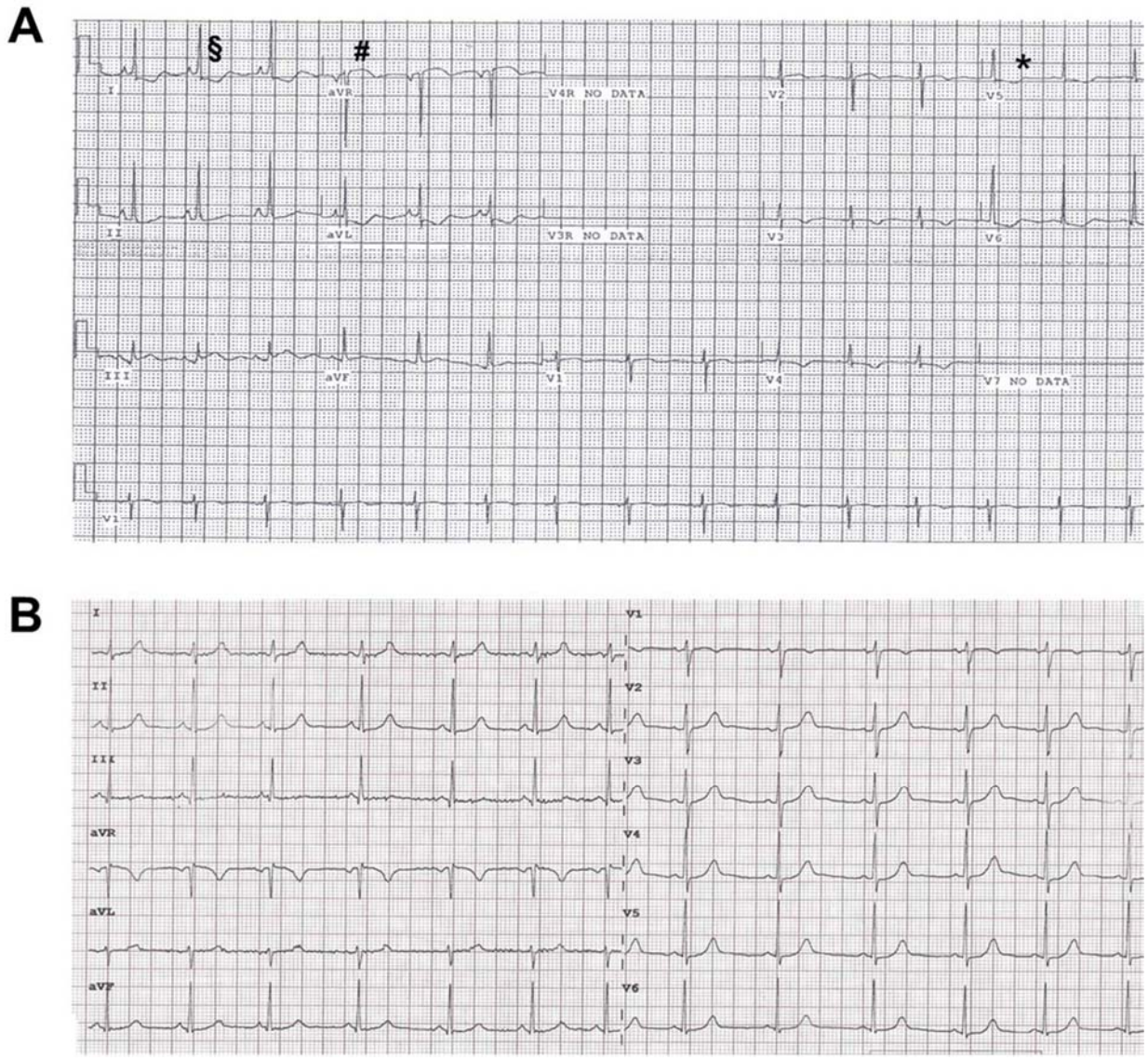

FIGURE S1. Electrocardiogram and rhythm strips in human subjects. Shown are representative 12-lead ECG recordings acquired at 25 mm/s. **(A)** Female HGPS patient (DB296; ECG #6) showing repolarization abnormalities such as negative and biphasic T waves (*), ST depression (§) and ST elevation (#). **(B)** Electrocardiogram tracing from a representative gender and age-matched healthy control (ID1)

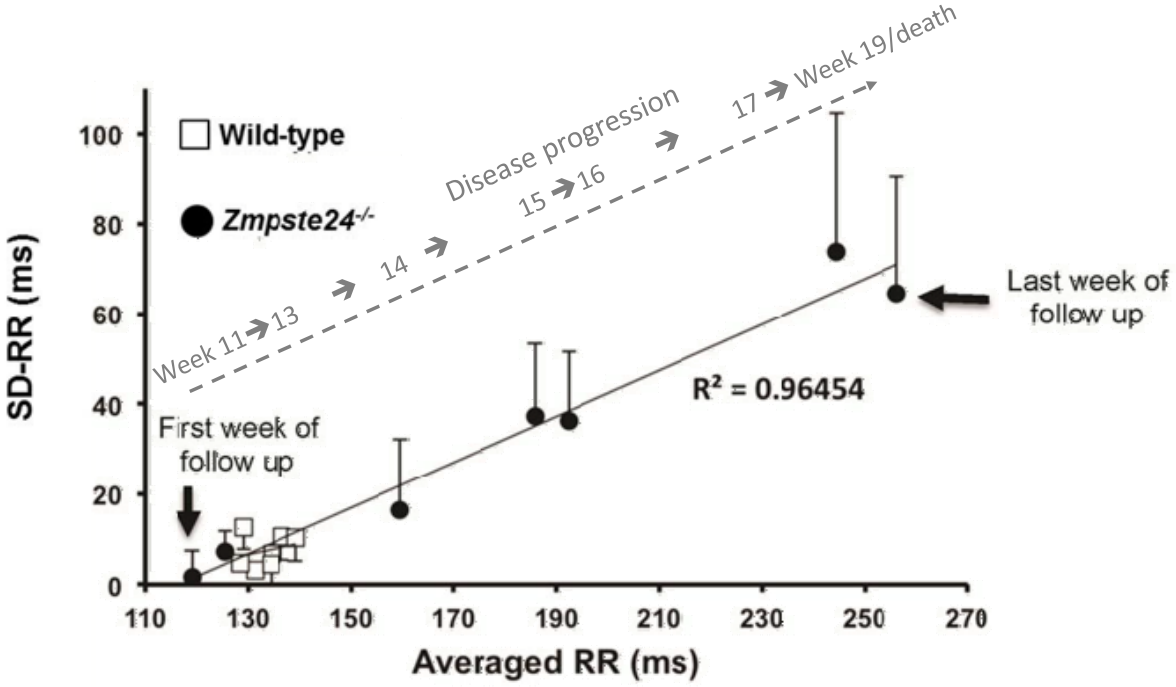

FIGURE S2. Linear increase of the R-R interval from the first to the last week of follow-up in *Zmpste24*$^{-/-}$ progeroid mice. WT and *Zmpste24*$^{-/-}$ mice were given weekly β-adrenergic challenge with isoproterenol starting at 11 weeks of age (First) and until 19 weeks of age or death of the animal (Last). Averaged RR and standard deviation RR (SD-RR) are shown in milliseconds (ms). The discontinuous line shows time progression as disease progresses from first week of follow up (11-13-week-old mice) until week 19 of age or death.

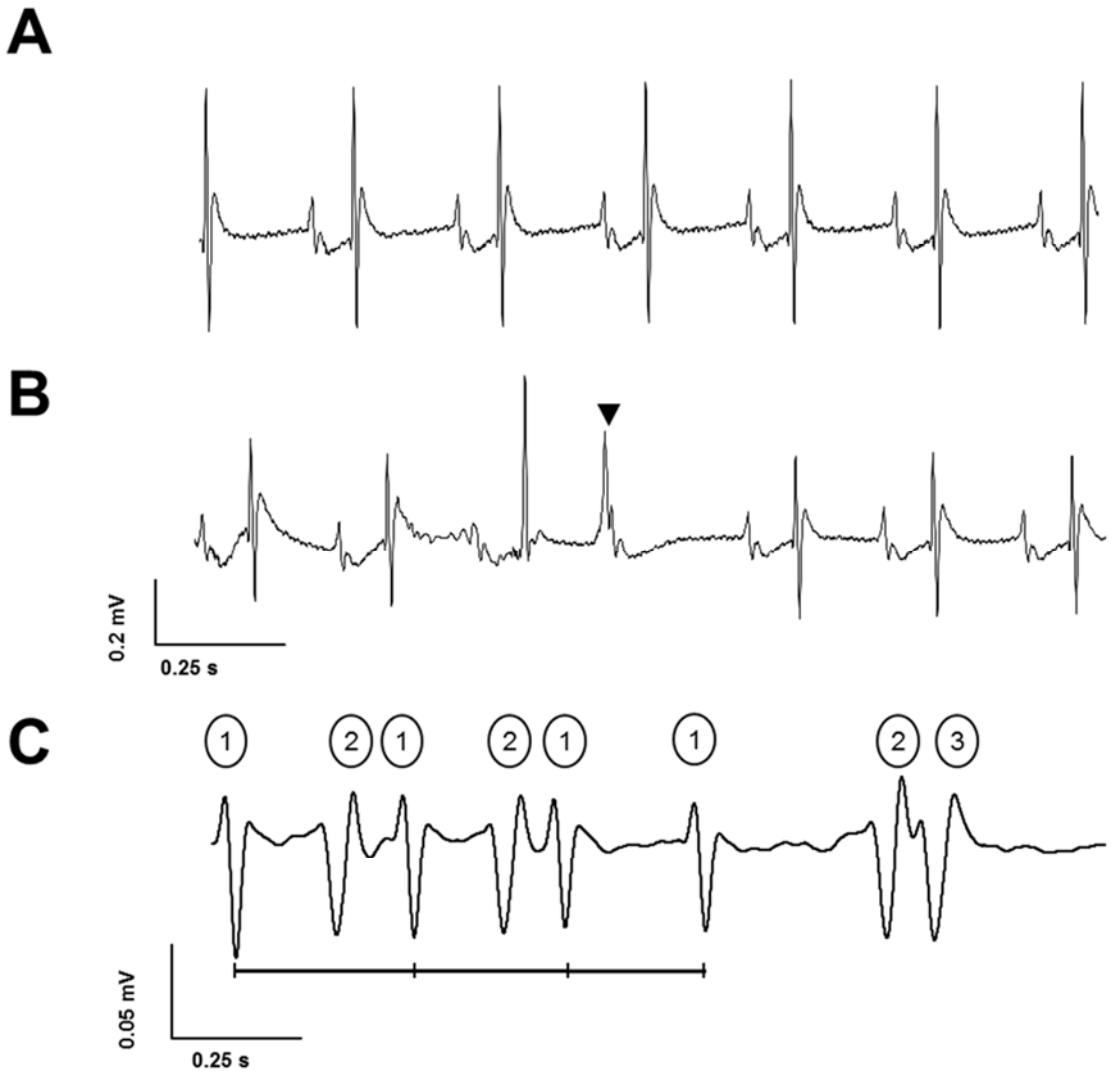

FIGURE S3. *Zmpste24*$^{-/-}$ mice develop premature ventricular complexes (PVC) and slow-rate polymorphic ventricular rhythms. Representative ECG traces and rhythm profiles recorded in lead aVF before **(A)**, after **(B)** and during recovery **(C)** of *Zmpste24*$^{-/-}$ mice from isoproterenol challenge at the last week of follow-up. Arrowhead indicates premature ventricular complexes. Different ventricular morphologies are indicated by numbers. At the beginning of the trace a pseudo-regular ventricular morphology seems to be present.

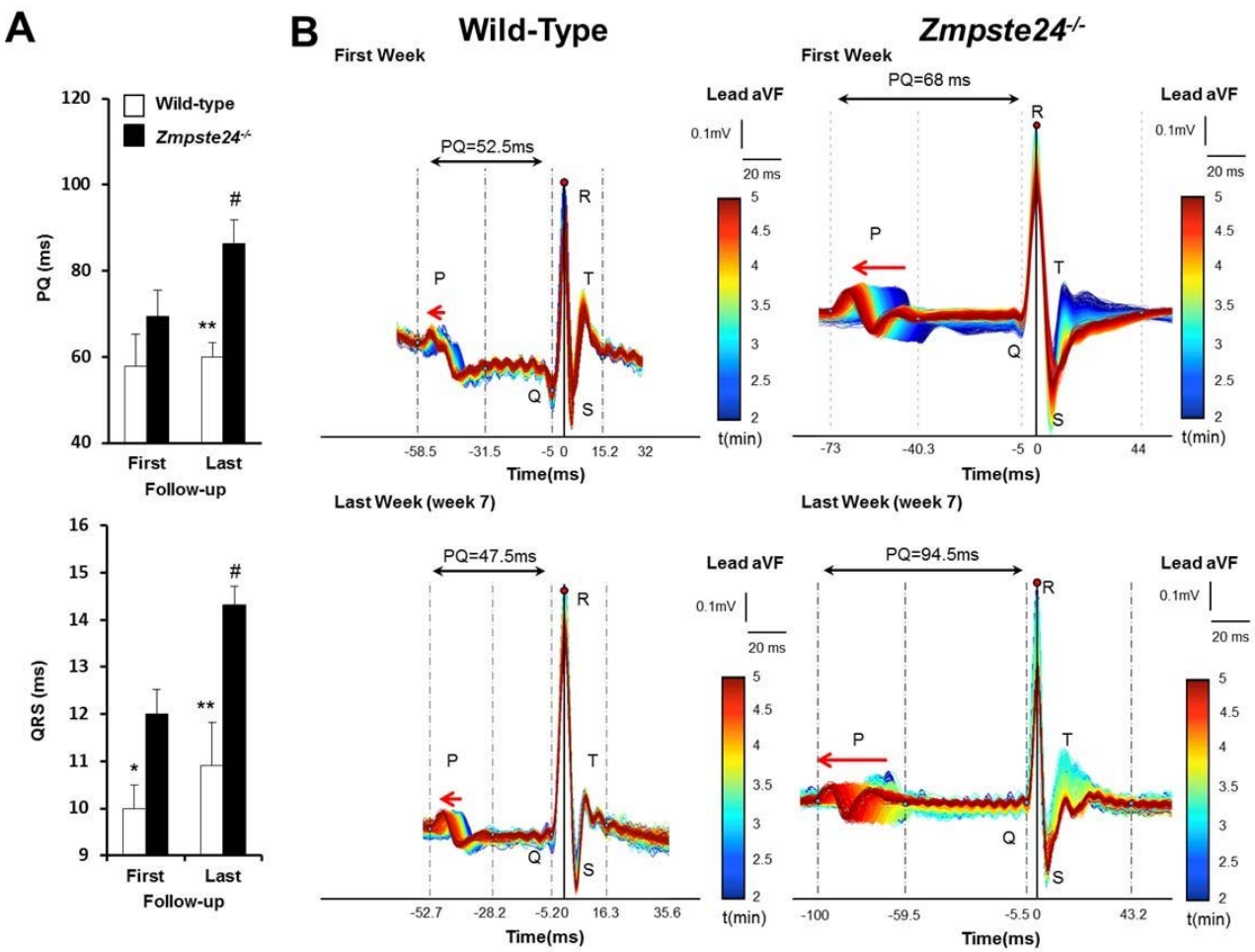

FIGURE S4. PQ and QRS abnormalities observed after isoproterenol bolus. WT and progeroid *Zmpste24*$^{-/-}$ mice were given weekly β-adrenergic challenge with isoproterenol starting at 11 weeks of age (First) and until 19 weeks of age or death of the animal (Last). **(A)** PQ and QRS quantification observed after the first isoproterenol challenge and after the last follow-up challenge. **(B)** Representative superimposed traces color-coded for time from blue to red, illustrating the time course of ECG changes in this period.

*, $p<0.05$; **, $p<0.01$; ***, $p<0.001$ (WT vs *Zmpste24*$^{-/-}$) .

#, $p<0.05$ (First vs Last week of follow-up).

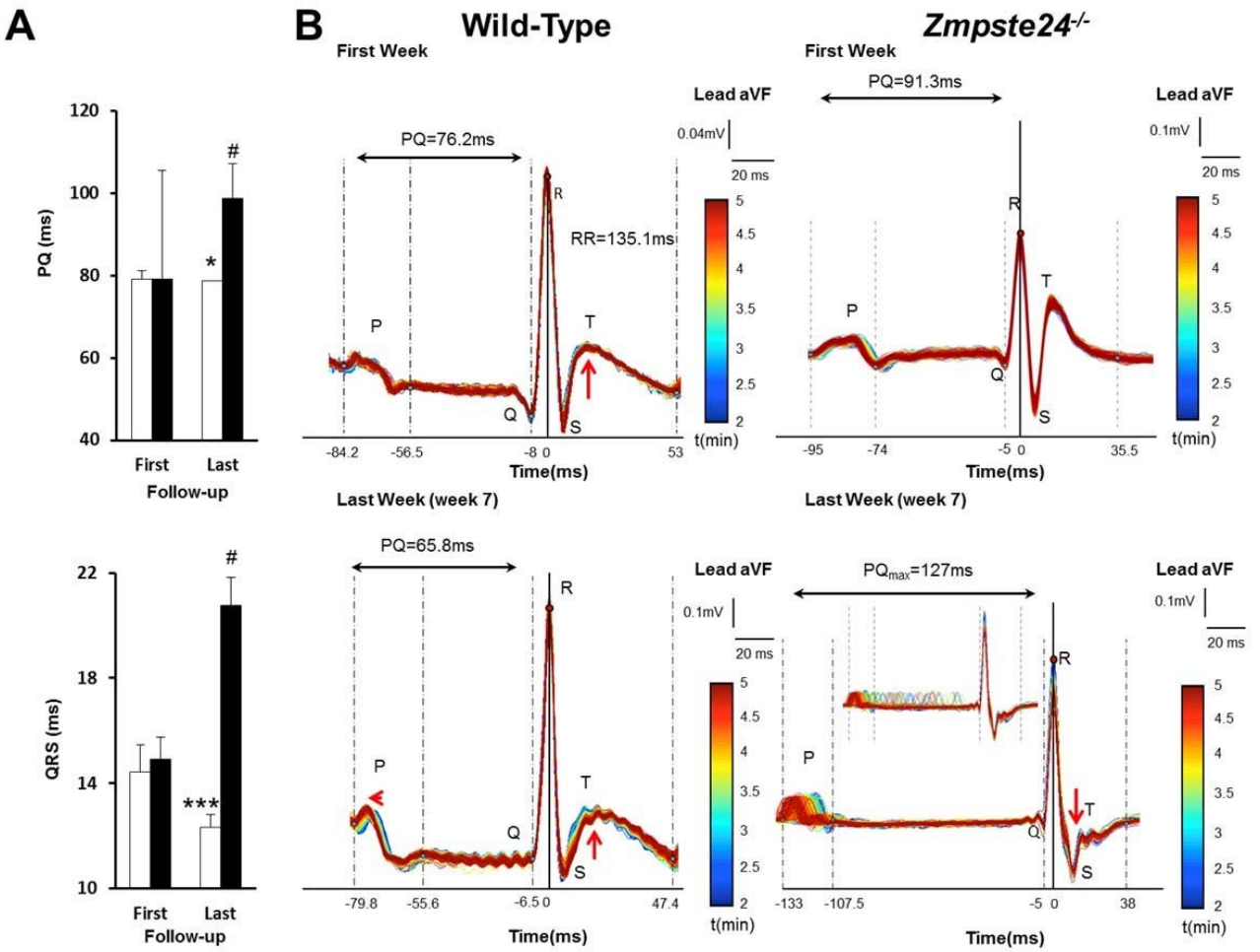

FIGURE S5. PQ and QRS abnormalities observed during recovery from isoproterenol. WT and progeroid *Zmpste24*$^{-/-}$ mice were given weekly β-adrenergic challenge with isoproterenol starting at 11 weeks of age (First) and until 19 weeks of age or death of the animal (Last). **(A)** PQ and QRS quantification observed during recovery after the initial first isoproterenol challenge and the last follow-up challenge. **(B)** Representative superimposed traces color-coded for time from blue to red, illustrating the time course of ECG changes in this period.

*, p<0.05; **, p<0.01; ***, p<0.001 (wild-type vs *Zmpste24*$^{-/-}$).

#, p<0.05 (First vs Last week of follow-up).

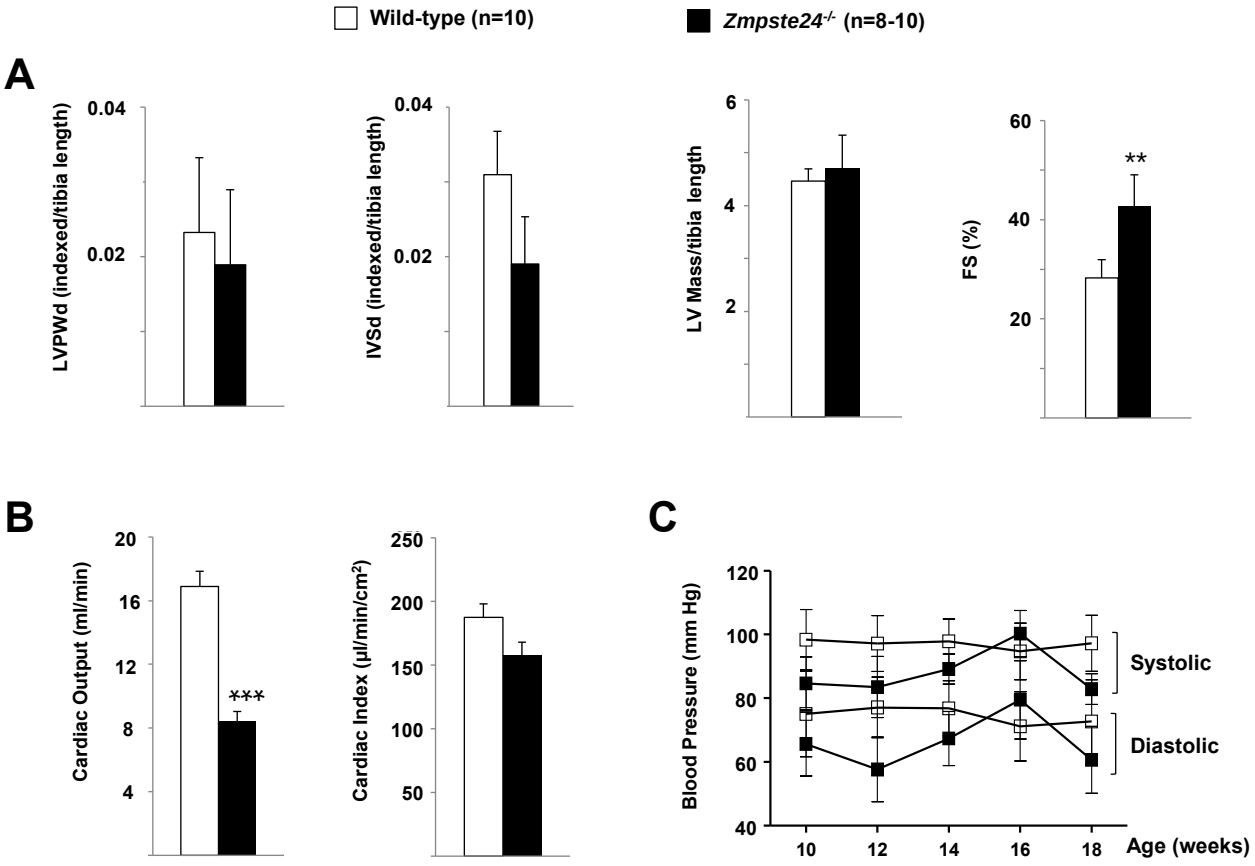

FIGURE S6. Progeroid *Zmpste24*$^{-/-}$ mice have preserved cardiac function and normal blood pressure. (A, B) Mice of both genotypes (18-20 weeks of age) were examined by trans-thoracic echocardiography to quantify LV posterior wall and interventricular septum thickness measured at diastole (LVPWd and IVSd, respectively), and LV mass. All LV parameters were corrected by tibia length. LV function is shown as fractional shortening (FS). Cardiac output (systolic volume x heart rate) and cardiac index (µl/min/cm^2) were also quantified. **(C)** Longitudinal analysis of mice of the indicated ages revealed no differences in blood pressure.

**, $p<0.01$; ***, $p<0.001$.

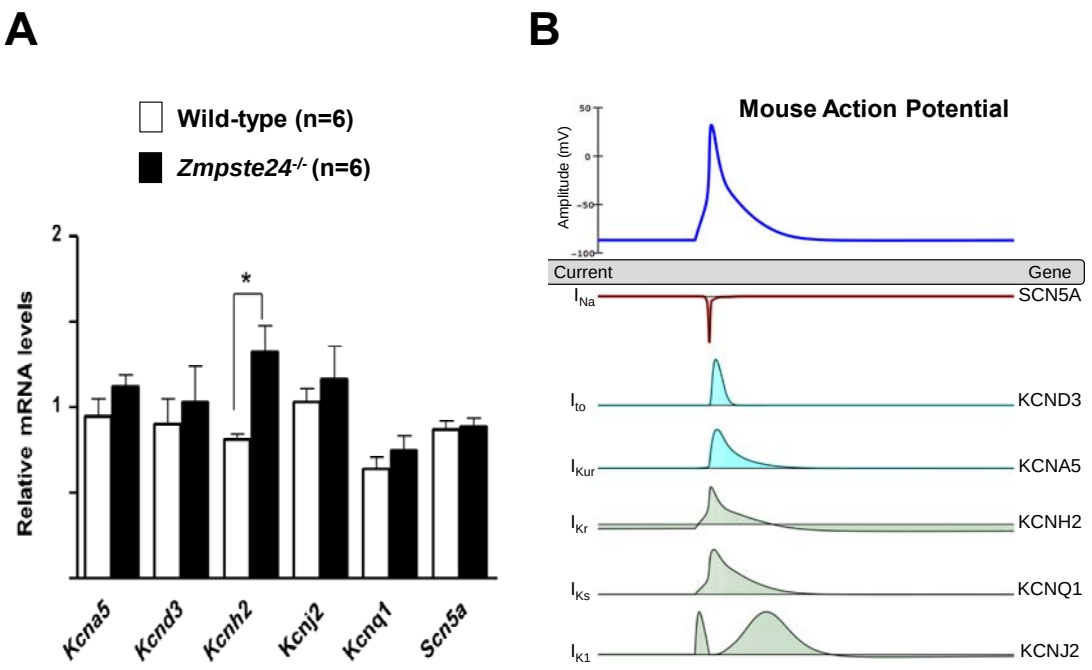

FIGURE S7. Expression of cardiac sodium and potasium channels in WT and *Zmpste24*$^{-/-}$ mice. (A) Real-time qPCR analysis in heart tissue from 16-18-week-old mice to examine mRNA levels of ion channels involved in the different phases of the action potential (see B). The graphs show relative mRNA transcript expression of the indicated sodium channel (*Scn5a*) and potassium channels (*Kcna5, Kcnd3, Kcnj2, Kcnq1, Kcnh2*). Results (Ct values) of triplicate samples from wild-type and progeroid *Zmpste24*$^{-/-}$ mice (n=6 per genotype) were normalized against 18S RNA and are presented as mean±SEM (relative to WT=1). *, $p<0.05$. **(B)** Representative mouse action potential obtained by computer simulation using the validated model reported by Li et al. (17), showing the participating ionic currents and their relation to the genes examined in this study. Elevated *Kcnh2* mRNA levels in *Zmpste24*$^{-/-}$ mice may explain the altered regulation of I_{kr} (rapidly-activated repolarizing potassium current), which might contribute to cardiac repolarization abnormalities.

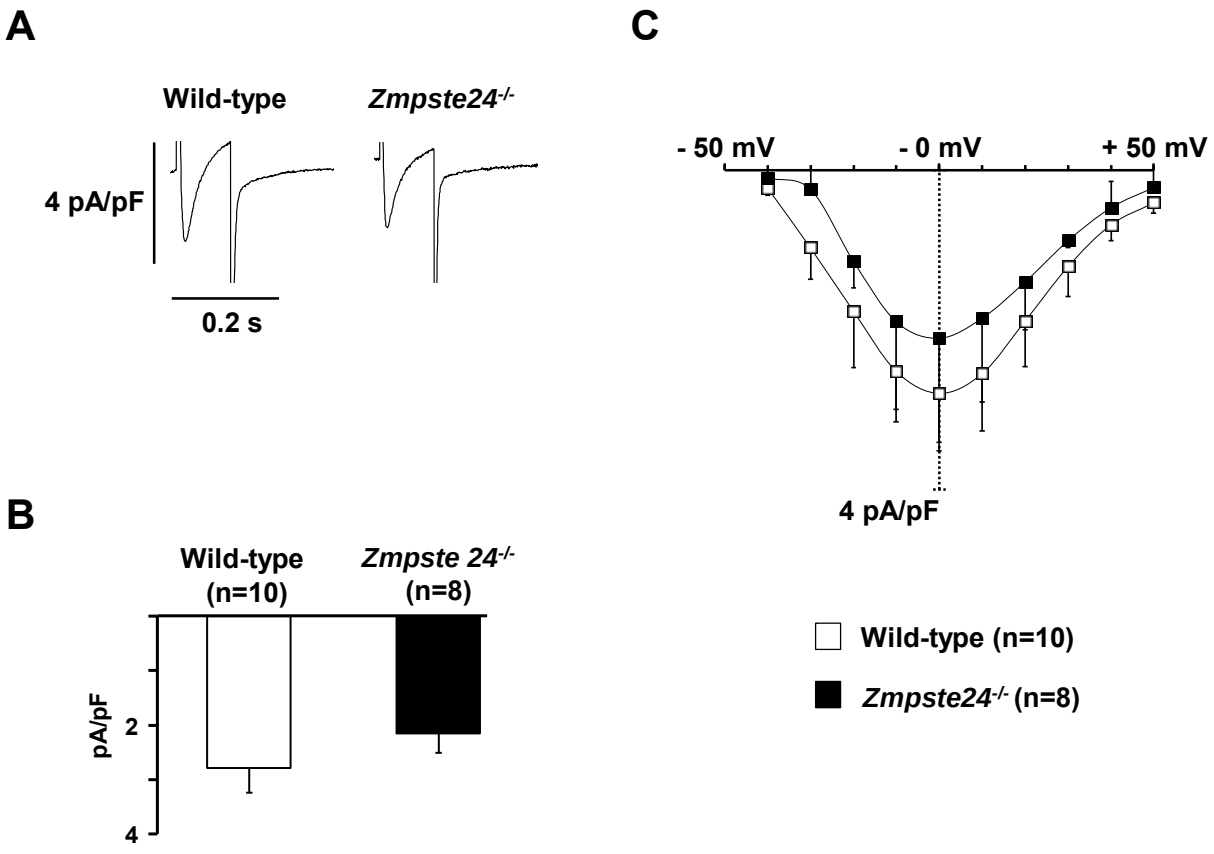

FIGURE S8. L-type calcium current is not significantly altered in *Zmpste24*$^{-/-}$ ventricular myocytes. (A) L-type calcium current traces recorded in myocytes stimulated at 0.5 Hz. **(B)** Average ICa amplitude in isolated myocytes stimulated continuously at 0.5 Hz. **(C)** ICa-voltage relationship recorded in the same myocytes.

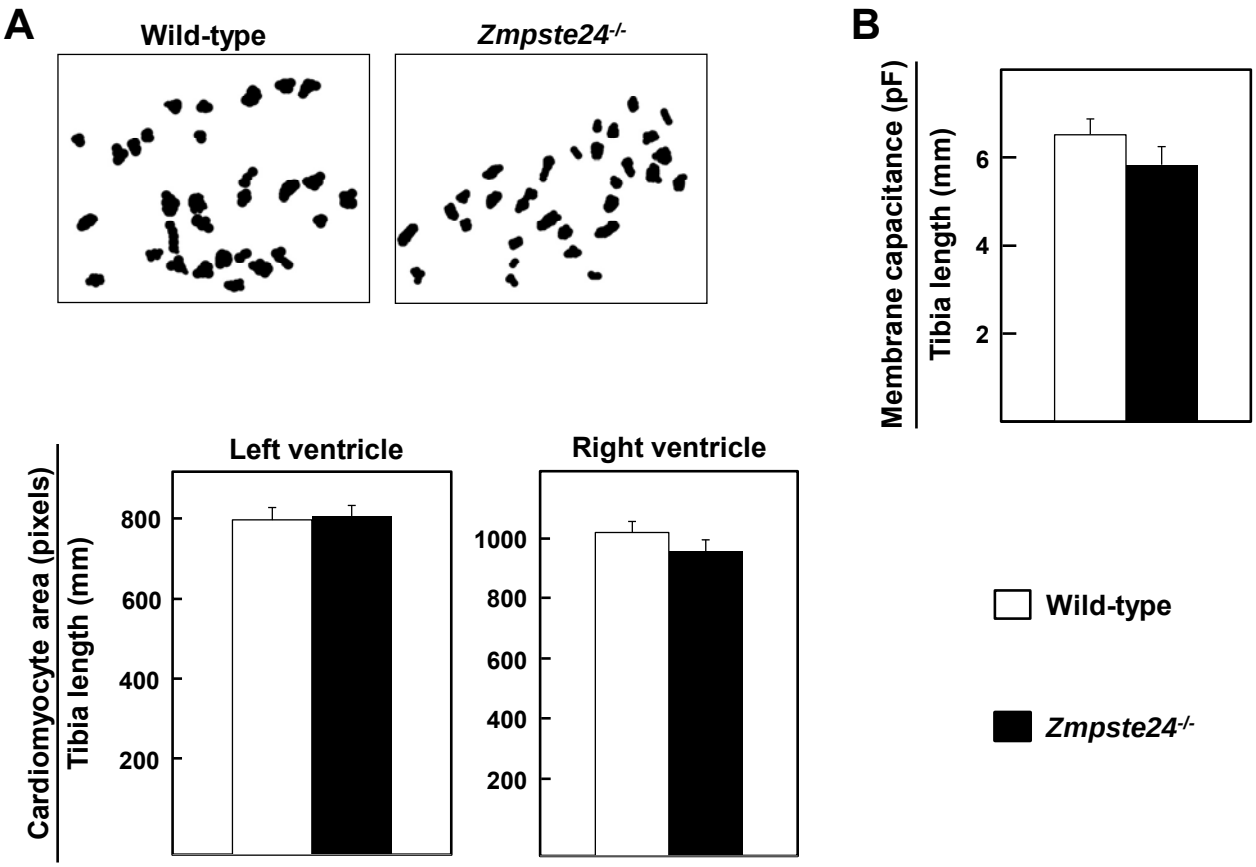

FIGURE S9. Cardiomyocyte size in wild-type and *Zmpste24*$^{-/-}$ mice. (A) Transverse sections of ventricular tissue of WT (n=4) and *Zmpste24*$^{-/-}$ (n=4) mice were stained with Mallory's trichrome or anti-laminin antibodies and digital images were analyzed with Adobe Photoshop to define the profiles of individual cardiomyocytes. **Top:** Representative examples of cardiomyocyte profiles. The total area of each cardiomyocyte cross section (as an estimate of the diameter/minor axis of the cells) was plotted as a black domain on a white background. **Bottom:** The profiles of 90 cardiomyocytes per ventricle (left and right) were analyzed with NIH J software to quantify cell surface (average number of pixels per cardiomyocyte). Graph bars indicate averaged number of pixels per cardiomyocyte normalized by tibia length. **(B)** Membrane capacitance of ventricular cardiomyocytes determined by patch-clamp was normalized by tibia length. Values are from n=23 cardiomyocytes from 10 *Zmpste24*$^{-/-}$ mice and n=39 cadiomyocytes from 12 WT mice. Results were normalized by tibia length because *Zmpste24*$^{-/-}$ mice are significantly smaller than age-matched WT controls. pF: picofarads.

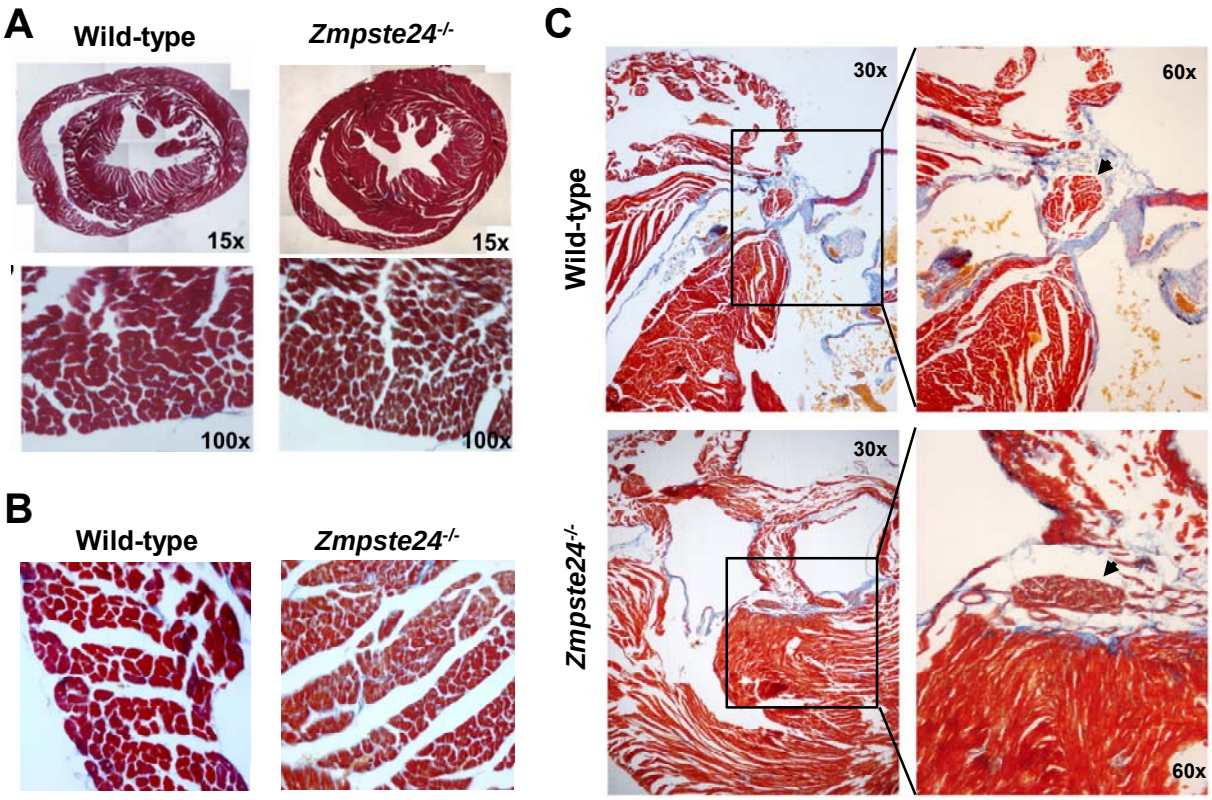

FIGURE S10. Immunohistopathological characterization of the heart of progeroid *Zmpste24*$^{-/-}$ mice. Heart cross-sections from mice at 18-20 weeks of age were stained with Mallory's trichrome. Five mice of each genotype were analysed and representative examples are shown. **(A, B)** Gross examination revealed normal morphology and myocardial fiber arrangement in the progeroid heart. Interstitial fibrosis was negligible in both genotypes. **(C)** Absence of fibrosis in the cardiac conduction system of progeroid *Zmpste24*$^{-/-}$ mice. Magnified views of selected areas are shown. Arrowheads indicate the atrio-ventricular node.

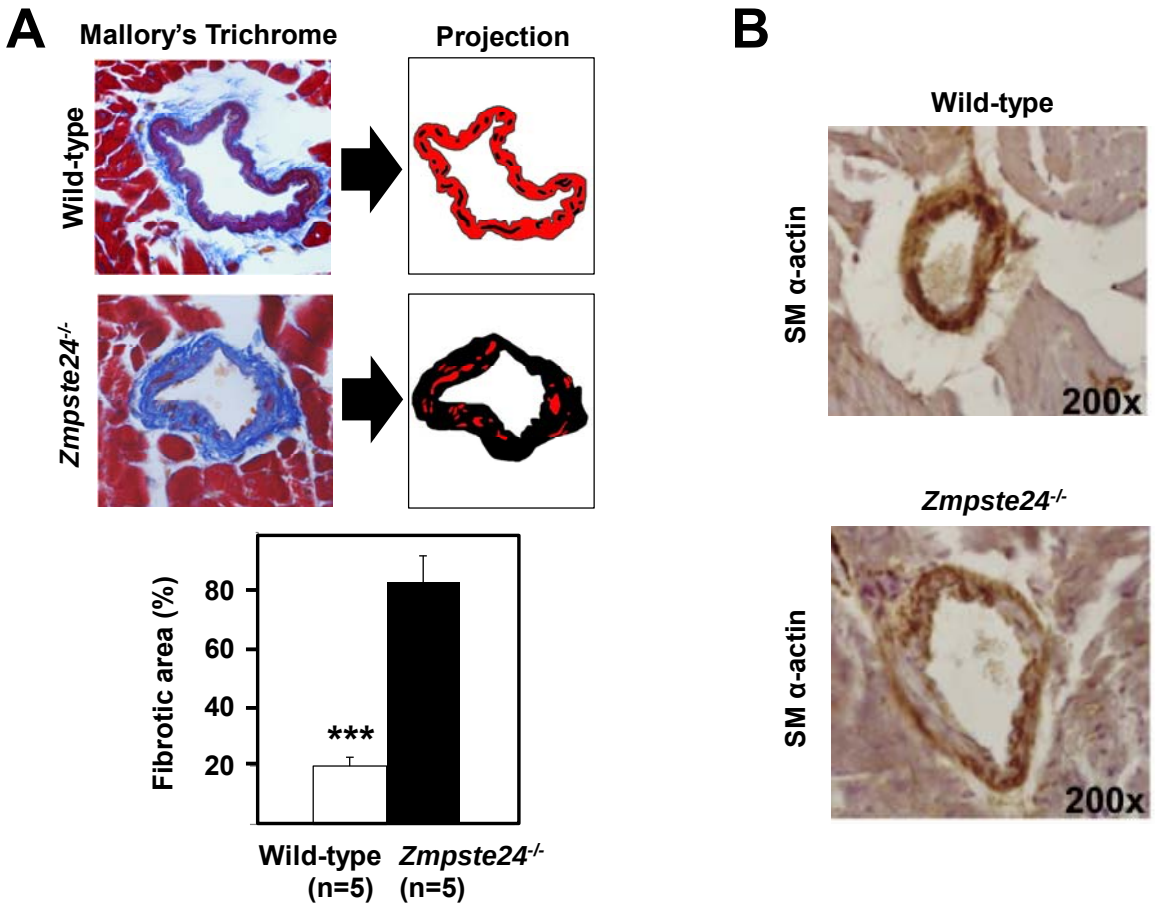

FIGURE S11. Abnormal coronary artery fibrosis in progeroid *Zmpste24*$^{-/-}$ mice. (A) To quantify coronary artery fibrosis, Mallory's trichrome-stained sections were analyzed (n=5 mice of each genotype). Large calibre arteries at the interventricular septum and free ventricular walls were identified and 3 transverse arterial profiles photographed along a total length of 300-400 µm (a minimal distance of 30 µm between sections was observed). Fibrotic and non-fibrotic areas in the vessel wall were projected using Adobe Photoshop (black: fibrotic area; red: non-fibrotic area), and the percentage of fibrotic pixels with respect to the total arterial surface was calculated with FiJi software. **(B)** Loss of smooth-muscle α-actin expression in the major coronary vessels of *Zmpste24*$^{-/-}$ mice.

***, $p<0.001$.

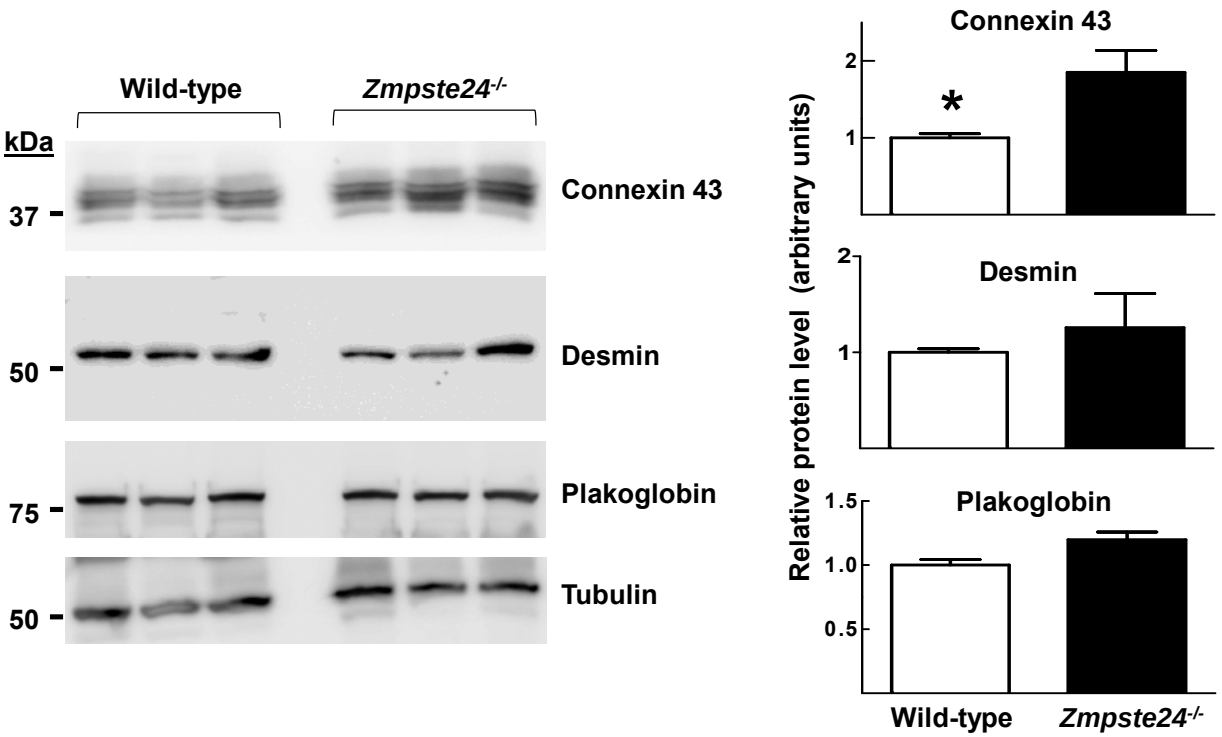

FIGURE S12. Increased expression of connexin 43 in hearts of progeroid *Zmpste24*$^{-/-}$ mice. **(A)** Representative western blots of gap junction proteins (connexin 43 and plakoglobin) and desmosome-interacting protein (desmin) in WT and *Zmpste24*$^{-/-}$ hearts (n=3 per genotype). Tubulin was used as a loading control. **(B)** Quantification of relative protein expression in progeroid mice, normalized to WT.

*, $p<0.05$.

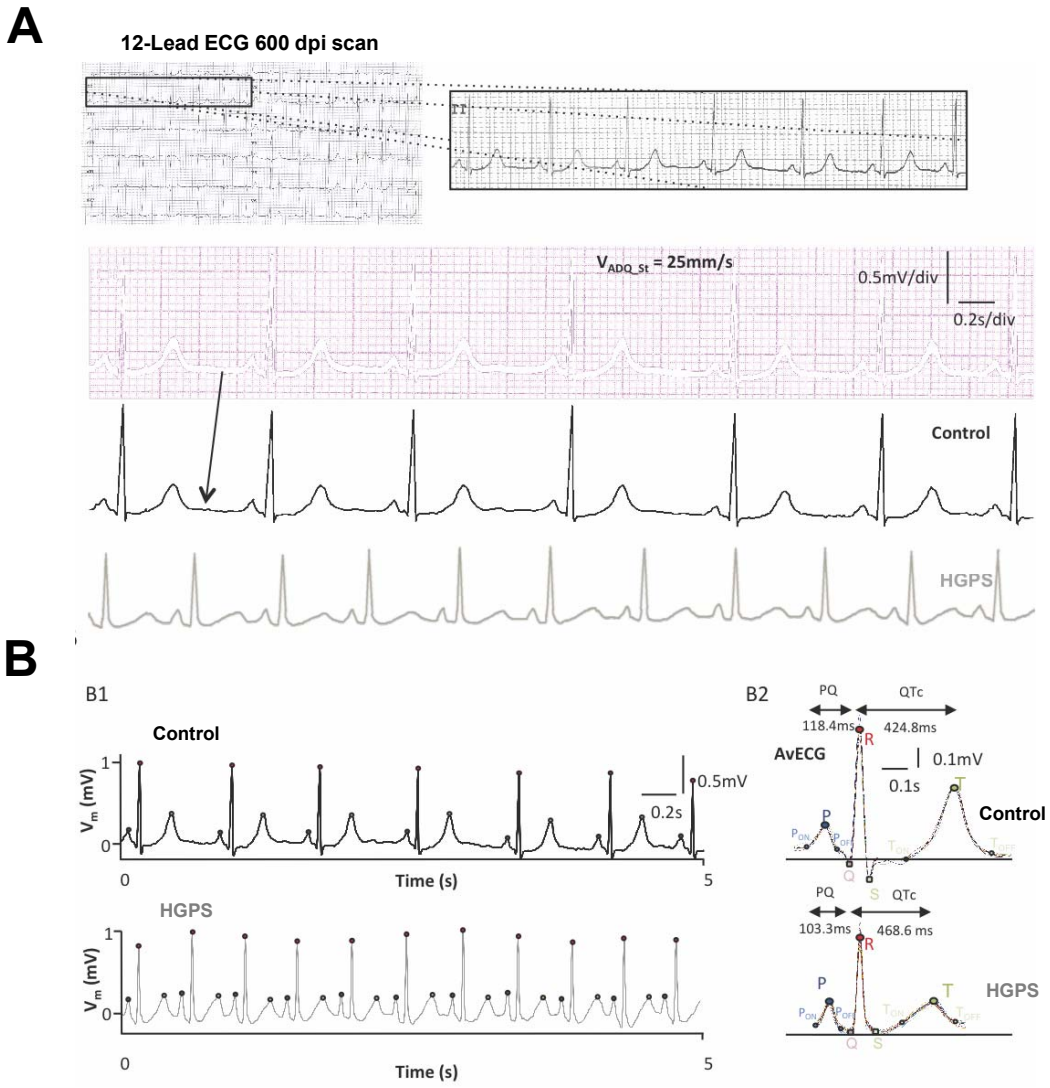

FIGURE S13. Extraction of electrocardiograms in human subjects. Representative 12-lead ECG recordings and extracted lead-II ECG acquired at 25 mm/s (controls in black and HGPS patients in gray). **(A)** Segmented and digitized traces. **(B)** Digitized signal (5-s segments) and averaged ECG calculation for feature extraction.

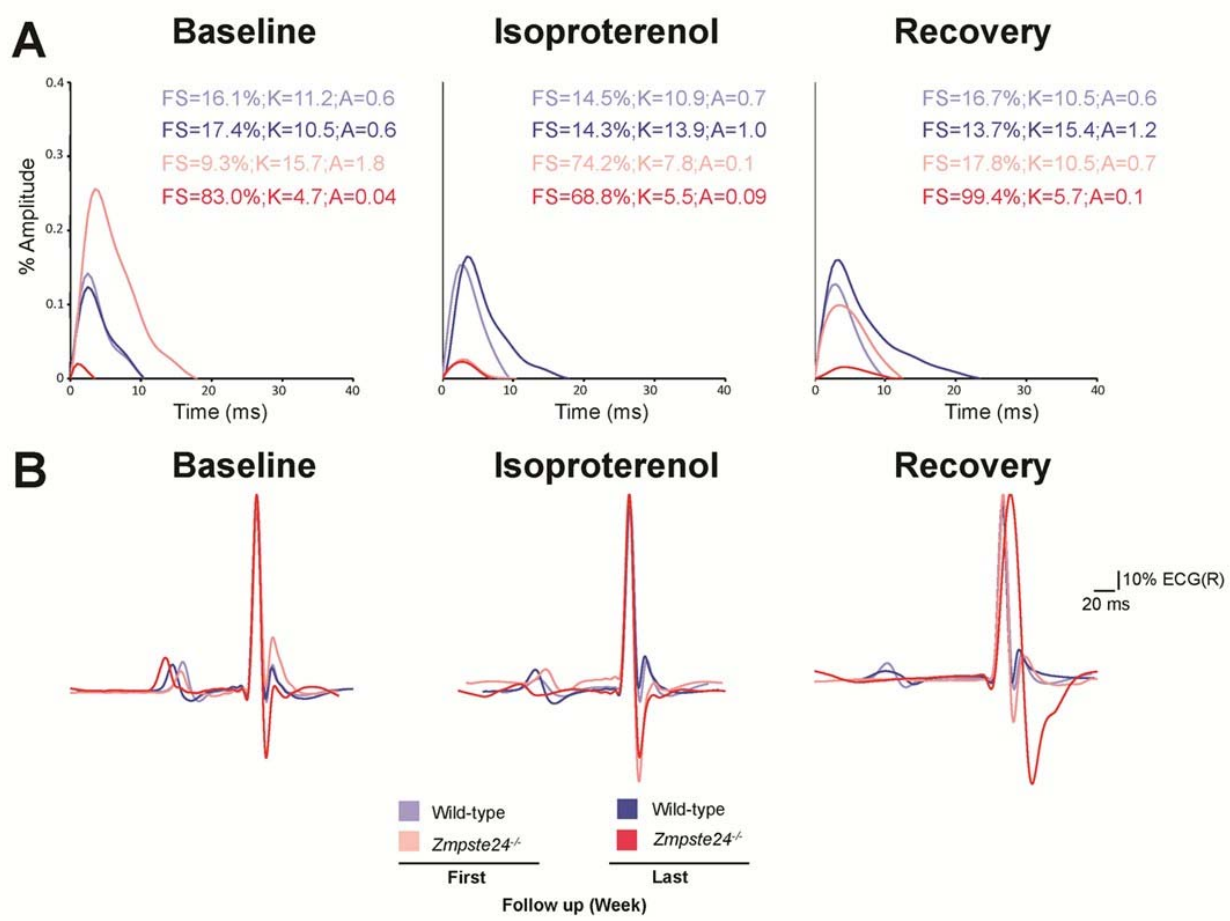

FIGURE S14. Sample measurement for mouse T-wave flattening estimation from normalized signal-averaged ECGs (SAECGs). (A) Segmented T-waves from T-onset to T_{90} and estimated flattening score, kurtosis and area under the T-wave. Increasing values of kurtosis and area under the T-wave correlate with decreasing values of flattening score in each time period. **(B)** SAECG traces obtained at baseline (immediately before isoproterenol), after isoproterenol, and during recovery. WT and *Zmpste24*$^{-/-}$ traces are color-coded in blues and reds, respectively, from light (initial) to intense (last week of follow-up).

TABLE S1. ELECTROCARDIOGRAPHIC MEASUREMENTS IN HGPS PATIENTS

ID	Gender	Age (Year/Month)	Weight (kg)	HR (bpm)*	QRS (ms)§	PR (ms)§	QTc (ms)#	REPOLARIZATION
DB001	**Female**							
ECG1		9Y 10M	11.8	110	74	120	402	Negative T wave V1,V2, aVL; Strain pattern DI
DB053¶	**Male**							
ECG1		13Y 5M	14.06	100	76	110	374	Negative T wave V1, V2, V3, aVL; Strain pattern DI
ECG2		13Y 7M	14.97	117	72	110	406	Negative T wave V1, V2, aVL; Strain pattern V3
ECG3		14Y 8M	14.52	118	72	110	382	Negative T wave V1, V2, V3, aVL; Strain pattern V4
ECG4		14Y 9M	14.97	84	80	115	377	Negative T wave V1, V2, V3
ECG5		15Y 4M	15.88	94	76	120	422	Negative T wave V1,V2,V3,aVL; ST Deppresion (1mm DI, aVL); ST Elevation (1 mm DIII, aVF); QV1-V4
DB060	**Male**							
ECG1		15Y 5M	19.65	88	90	100	388	No repolarization abnormalities
ECG2		16Y 1M	21.85	69	90	110	413	Negative T wave V1; Strain Pattern aVL
DB071	**Male**							
ECG1		16Y 8M	19.5	95	80	140	360	No repolarization abnormalities
ECG2		17Y 8M	18.7	83	80	120	401	ST Depression (2mm V5-V6 (biphasic T wave); 1 mm DI, aVL)
ECG3		17Y 8M	18.7	97	80	120	450	ST Depression (2mm V5,V6 (biphasic T wave); 1 mm DI, aVL)
DB073	**Male**							
ECG1		7Y 2M	9.98	116	70	120	418	Negative T wave V1, V2, V3; Strain pattern V4, aVL
ECG2		7Y 9M	10.21	111	70	125	408	Negative T wave V1, V2, V3; Strain pattern V4
DB100	**Male**							
ECG1		11Y 4M	10.7	107	95	130	428	Q wave DIII
ECG2		11Y10 M	11.57	133	90	125	417	Q wave DIII
DB110	**Female**							
ECG1		6Y 11M	10.9	111	66	116	435	Negative T wave V1, V2
ECG2		7Y 8M	10.5	79	77	120	367	Negative T wave V1, V2
ECG3		8Y 3M	10.9	107	76	120	428	Negative T wave V1, V2, V3; Strain Pattern V4
ECG4		8Y 10M	11	88	76	115	376	Negative T wave V1, V2, V3; Strain Pattern V4
ECG5		9Y 1M	11.2	111	80	120	422	Negative T wave V1, V2, V3; DIII
ECG6		9Y 3M	10.94	88	90	130	412	Negative T wave V1,V2,V3 ; Strain pattern DII
DB113	**Female**							
ECG1		10Y	13.15	150	70	100	395	No repolarization abnormalities
DB118	**Male**							
ECG1		5Y 7M	12.5	150	79	110	427	Negative T wave V1, V2, DII, DIII

ECG2		6Y 4M	11	103	76	125	433	Negative T wave V1,V2, V3; Strain Pattern DIII, V4
ECG3		7Y	11	139	83	125	442	Negative T wave V1,V2, V3, DIII
ECG4		7Y 11M	11.5	79	75	120	379	Negative T wave V1,V2, V3; Strain Pattern V4
ECG5		8Y 5M	11	75	72	120	402	Negative T wave V1,V2, V3, V4, V5
DB120	**Male**							
ECG1		12Y 1M	13.3	115	85	130	388	Negative T wave V1, aVL; Strain Pattern V2
ECG2		13Y 11M	13.3	142	80	120	370	ST Depression (1 mm DI, DIII, aVF; 2 mm DII, V5-V6 (biphasic T wave)); ST elevation (2 mm aVR)
DB136	**Male**							
ECG1		1Y 9M	5.44	136	60	100	347	Negative T wave V1, V2,V3; DIII; Strain Pattern aVF
DB138	**Male**							
ECG1		15Y 11M	17.2	107	90	120	401	Negative T wave aVL; ST Depression (1 mm V4,V5,V6, DI)
ECG2		16Y 1M	18	97	90	130	406	Negative T wave aVL; ST Depression (1 mm V4,V5, DI, aVL)
ECG3		16Y 1M	18	100	90	130	413	Negative T wave aVL; ST Depression (2 mm V4,V5, 1mm V6, DI, aVL)
ECG4		18Y	17.9	133	100	190	537	ST Depression (4 mm V4, V5-V6 (biphasic T wave), 2 mm DI,DII, aVL); ST Elevation (2 mm aVL, V1)
DB145	**Female**							
ECG1		16Y 9M	13.06	107	82	120	401	Strain Pattern V1, aVL
ECG2		17Y 2M	13.22	94	76	120	388	Negative T wave V5, V6; Strain Pattern DIII, aVF, V1, V4
ECG3		18Y 5M	12.93	100	80	120	374	Negative T wave V5, V6; Strain Pattern aVL, V1, V4
ECG4		18Y 5M	12.93	101	80	120	378	Negative T wave V3,V4, V5 ; Strain Pattern aVL, DI,V6
ECG5		19Y	14.15	115	80	130	444	Strain Pattern aVL, aVF, DIII,V4; ST Depression (1mm; V5, V6, DII)
ECG6		19Y 5M	13.64	100	80	120	413	Negative T wave V4, V5, aVL ; Strain Pattern V3, aVF, DI, DII
DB244	**Male**							
ECG1		9Y	10.61	97	72	120	406	Negative T wave V1
ECG2		9Y 4M	10.4	120	72	120	424	Negative T wave V1,V2; Strain Pattern DIII
ECG3		9Y 10M	10.6	130	75	120	398	Negative T wave V1,V2, DIII; Strain Pattern V3
ECG4		10Y 7M	11.1	115	75	120	416	Negative T wave V1,V2; Strain Pattern DIII, V3
ECG5				122	75	120	443	Negative T wave DIII; V1; Strain Pattern aVF
DB296	**Female**							
ECG1		10Y 8M	6.77	127	70	110	462	Negative T wave V1, V3; Strain pattern DIII, aVF
ECG2		10Y 8M	6.77	114	70	100	416	Negative T wave V1, V2; Strain pattern DIII
ECG3		10Y 8M	6.77	112	72	95	440	Negative T wave V1, V2
ECG4		11Y 10M	7.65	133	70	100	472	ST Depression (3 mm V3, V4, V5, V6; 2 mm DI , DII, 1mm DIII); ST elevation (2mm aVR)
ECG5		11Y 11M	7.19	100	70	100	443	Negative T wave V1, V2, V3; ST Depression (1mm V3, V4, V5, V6, DI, aVL); ST elevation (1mm aVL)
ECG6		12Y 5M	7.25	96	70	100	382	Negative T wave V3; V4, V5-V6 (biphasic T wave); ST Depression (1mm DI-DII); ST Elevation (1mm aVR)

* HR: Heart rate (expressed in beats per minute: bpm)

§ QRS, PR and repolarization abnormalities based on age-related changes in pediatrics.

Normal QTc for the adult population is <450 ms and <470 ms in men and women respectively

¶ Denotes overt pathological ECGs

TABLE S2. ELECTROCARDIOGRAPHIC MEASUREMENTS IN HEALTHY CONTROLS

ID	Gender	Age (Years)	Weight (kg)	HR (bpm)*	QRS (ms)	PR (ms) §	QTc (ms)	REPOLARIZATION
1	**Female**	13	61	70	80	115	431	Negative T wave V1; Strain pattern DIII
2	**Female**	7	22	96	70	135	457	Negative T wave V1; Strain pattern V2
3	**Female**	14	64	113	75	100	385	Negative T wave V1,V2,V3
4	**Male**	19	92	59	100	120	396	Negative T wave V1; Strain Pattern aVL
5	**Male**	19	75	59	100	150	376	No repolarization abnormalities
6	**Male**	18	75	67	85	125	392	No repolarization abnormalities
7	**Female**	9	29	67	85	125	390	Negative T wave V1; Strain Pattern DIII
8	**Female**	7	23	74	80	130	389	Negative T wave DIII
9	**Male**	6	20	86	73	140	430	Negative T wave V1,V2; Strain Pattern aVL
10	**Male**	5	19	79	76	113	413	Negative T wave V1
11	**Female**	6	22	87	82	120	421	Negative T wave V1,V2
12	**Female**	8	33	109	80	120	431	Negative T wave V1,V2,V3
13	**Female**	4	18	67	85	120	358	Negative T wave V1

* HR: Heart rate (expressed in beats per minute: bpm)
§ Normal PR is <200 ms
# Normal QTc for the adult population is <450 ms and <470 ms in men and women respectively

TABLE S3. Surface ECG analyses comparing fundamental rhythm parameters between WT and *Zmpste24*$^{-/-}$ mice

	Wild-type (n=6)			*Zmpste24*$^{-/-}$ (n=6)		
Parameters (ms)	**Baseline**	**ISO**	**Recovery**	**Baseline**	**ISO**	**Recovery**
			First week of Follow-Up			
RR	155.85 ± 13.52	131.99 ± 7.23	136.98 ± 4.43	176.73 ± 20.08	136.08 ± 7.22†	210.68 ± 19.89**
PQ	49.16 ± 1.44	57.83 ± 7.36	79.25 ± 4.25†††	53.58 ± 5.03	69.31 ± 6.11†	72.48 ± 19.23†††
QRS	10.80 ± 0.23	10.00 ± 0.48	14.41 ± 1.03††	13.83 ± 1.18*	12.00 ± 0.51*	14.91 ± 0.81
QTc_{90}	25.37 ± 2.07	20.61 ± 1.51†	37.69 ± 5.37	24.61 ± 1.54	24.55 ± 0.56*	25.77 ± 0.91*
			Last week of Follow-Up			
RR	129.73 ± 6.24	119.43 ± 3.47	137.96 ± 2.58	240.37 ± 37.12*	201.41 ± 50.19** ‡	301.59 ± 29.51***‡
PQ	45.66 ± 3.01	60.01 ± 3.34††	78.66 ± 3.78†††	67.41 ± 6.19*	86.34 ± 5.44*** †‡	98.75 ± 8.46* †‡
QRS	10.5 ± 0.32	10.91 ± 0.92	12.33 ± 0.47†	13.9 ± 1.37*	14.31 ± 0.41** ‡‡	20.75 ± 1.07*** ††‡
QTc_{90}	21.83 ± 2.38	22.36 ± 3.19	23.24 ± 4.61	25.52 ± 2.14	24.25 ± 2.03	24.53 ± 2.17

*, P<0.05; **, P<0.01; ***, P<0.001 (Wild-type vs *Zmpste24*$^{-/-}$)

†, P<0.05; ††, P<0.01; †††, P<0.001 (vs Baseline)

‡, P<0.05; ‡‡, P<0.01; P<0.001 (‡ First vs Last week of follow-up)

Mice were given a weekly β-adrenergic challenge with isoproterenol starting at 11 weeks of age (First week of Follow-Up) and until 19 weeks of age or death of the animal (Last week of Follow-Up). Surface ECG analyses comparing fundamental rhythm parameters were performed in anesthetized WT and *Zmpste24*$^{-/-}$ mice at baseline, after adrenergic challenge with isoproterenol (ISO) and during recovery.

TABLE S4. Electrophysiological parameters of transmembrane action potentials recorded ex vivo in ventricular multicellular preparations

Tissue	Mice (n=5)	BCL (ms)	Frequency (Hz)	RMP (mV)	Vmax (V/s)	APA (mV)	APD_{20} (ms)	APD_{50} (ms)	APD_{90} (ms)
Right ventricle	Wild-type	258±31	4.8±0.6	-80.1±1.9	231±10	115.8±2.5	11.6±2.1	35.9±6.2	126±14
	Zmpste24 $^{-/-}$	265±26	4.2±0.5	-77.1±1.2	217±17	117.3±1.9	12.7±1.1	41.3±1.7	120±6
Left ventricle	Wild-type	Stimulated	3	-77.6±1.0	229±3.5	121.5±1.7	9.6±0.7	41.3±1.9	136±7
	Zmpste24 $^{-/-}$	310±24	3.2±0.2	-82.8±2.5	260±7.4	121.2±1.2	13.3±1.2	39.4±2.6	121±5

BCL: Basic cycle length expressed in milliseconds (ms)

RMP: Resting membrane potential expressed in millivolts (mV)

Vmax: Maximum velocity of depolarization

APA: Action potential amplitude

APD: Action potential duration measured at indicated % of repolarization and expressed in ms